JOURNAL OF SPACECRAFT AND ROCKETS
Vol. 39, No. 1, January–February 2002

New Failure Criterion for Space Shuttle Main Engine Turbine Blades

M. Tarek Sayyah*
Sverdrup Technology, Inc., Huntsville, Alabama 35814
and
William P. Schonberg†
University of Missouri–Rolla, Rolla, Missouri 65409

The orientation of a single-crystal material is known to affect the strength and life of structural component parts. Results are presented of an investigation of the effects of secondary axis orientation angles on the failure of the first-stage of the space shuttle main engine alternate turbopump development of the high-pressure fuel turbopump. First, the correlation of different failure models with low-cycle fatigue data for nickel-base single-crystal test specimens was analyzed. Then the models with the highest correlation coefficients were used to study the actual single-crystal blade structure. Based on the results obtained, a new failure model was proposed. A detailed finite element model for the first-stage blade was used to calculate the stresses and strains at all blade nodes for different material orientations. Results of the analysis showed that the critical value of the failure model could vary by up to a factor of 3 by changing the primary and secondary material orientations. A comparison between analytical results and engine test results showed good correlation and also demonstrated the dependence of cracking location on crystal orientation.

Nomenclature

E	=	material Young's modulus, N/m^2
$f(N)_{1,\ldots,6}$	=	critical failure model values
K, S	=	empirical constants found by fitting fully reversed torsion data to fully reversed uniaxial data
N	=	number of loading cycles to failure initiation
R^2	=	correlation coefficient
V_0	=	critical value of the strain-energy density, J/kg
γ	=	primary material angle relative to casting x axis, deg
$\gamma_{\max}$, $\Delta\gamma_{\max}$	=	maximum shear strain amplitude
γ_{xy}, γ_{yz}, γ_{zx}	=	generic shear strains
Δ	=	primary material angle relative to casting y axis, deg
$\varepsilon_{\max}$	=	maximum strain normal to a slip plane
ε_n, $\Delta\varepsilon_n$	=	normal strain amplitude
ε_x, ε_y, ε_z	=	generic normal strains
θ	=	secondary material angle relative to casting z axis, deg
$\sigma_{\max\text{-}n}$	=	maximum normal stress, N/m^2
σ_n	=	stress normal to the maximum shear strain plane, N/m^2
σ_x, σ_y, σ_z	=	generic normal stresses, N/m^2
σ_{ys}	=	material yield strength, N/m^2
τ_{xy}, τ_{yz}, τ_{zx}	=	generic shear stresses, N/m^2

Introduction

THE new generation of the space shuttle main engine (SSME) high-pressure turbomachinery is known as the alternate turbopump development (ATD) hardware. These turbines have undergone rigorous hot-fire testing, including component evaluation at the Pratt and Whitney E8 hot-gas full-scale engine testing facility and certification at the NASA Stennis Space Center (SSC). This advanced hardware includes new high-pressure fuel turbopumps (HPFTP) and new high-pressure oxygen turbopumps (HPOTP). The current SSME turbopumps, though not without a few problems, have proven to be quite reliable even though they were basically designed and built 25 years ago. The aerospace community has long felt that new high-pressure turbines should be designed that would take advantage of the latest technology in materials and analysis and that could use the knowledge gained from experience with the current SSME hardware.

One area in which new materials technology has been applied to ATD hardware is in the use of single-crystal superalloy materials. Single-crystal superalloys were identified as potential blade materials that warranted further development for advanced liquid-propellant rocket engine turbopumps.[1] As part of this development, materials scientists have evaluated the mechanical properties of several single-crystal superalloys in an attempt to find a suitable candidate replacement blade material for the SSME turbopumps and for other advanced rocket engines.[2,3] A well-characterized single-crystal face-centered cubic nickel superalloy (PWA 1480) has recently been selected by Pratt and Whitney as the blade material for the ATD program for the SSME. This material is known for its high-temperature strength, high fatigue life, and improved resistance to property deterioration in the presence of hydrogen. Both newly designed turbopumps, the HPFTP and the HPOTP, now employ this material for the casting of the turbine blades.

Turbine blades of nickel-base single-crystal superalloys (including PWA 1480) are typically directionally solidified along the low modulus [001] crystallographic direction to enhance thermal fatigue resistance. This directional solidification generates a secondary crystallographic direction [010] that is randomly oriented with respect to fixed geometric axes in the turbine blade. However, using a seed crystal during solidification can control the orientation of the secondary crystallographic direction.[4] Because single-crystals exhibit anisotropic elastic behavior, the stress-strain response and dynamic characteristics of a turbine blade that is directionally cast along the [001] crystal orientation can vary with the orientation of the secondary crystallographic direction within the blade.[5,6]

During the casting process of the single-crystal blades, the crystallographic orientation is currently controlled only for one axis of the crystal. Specifically, the primary axis must be within a 15-deg cone of the blade-staking axis while the orientations of the other

Received 10 August 2000; revision received 13 August 2001; accepted for publication 18 August 2001.

*Structural Engineer, P.O. Box 11541.
†Professor and Chair, Civil Engineering Department, 1870 Miner Circle; wschon@umr.edu. Associate Fellow AIAA.

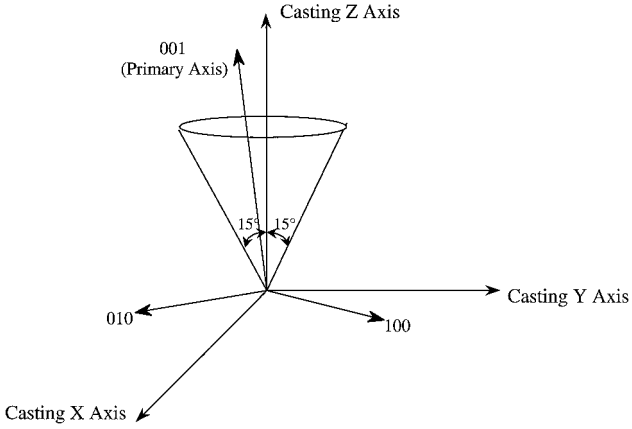

Fig. 1 Primary-axis orientation with respect to the stacking axis.

crystallographic axes are uncontrolled (see Fig. 1). Recent engine test results obtained using the two ATD/HPFTP constructions and performed at NASA SSC showed that the first- and second-stage blades for the HPFTP were experiencing cracks. These cracks were found in the airfoil tips in multiple blades, and a few cracks grew all of the way across the wall of the hollow-core airfoil. Those cracks that grew across the wall propagated down the length of the blade and, in one case, failed the blade, causing damage to the ATD/HPFTP and the SSME. A number of analytical studies[7–9] were performed to address the concern that these cracks could result because the secondary axes of the ATD/HPFTP turbine blades were not controlled during the single-crystal solidification process. These studies typically found that the stress fields within the blades were strongly dependent on the orientations of the nonprimary crystallographic axis.

Based on the engine test results as well as those obtained from these studies, it became evident that uncontrolled secondary material axis orientations can cause stress uncertainties in ATD/HPFTP turbine blades, which in turn could lead to blade cracking. Currently, no methodology exists that predicts crack growth for a single-crystal material or any other material with orthotropic properties in a complex loading environment. As a result, a new approach needs to be developed, based on available fatigue and fracture test data, for predicting the influence of the secondary orientation angles on the behavior of the single-crystal materials. This paper presents the results of a study whose goal was to develop a new failure model that would be applicable in predicting the influence of both primary and secondary material orientations on the behavior of the first stage single-crystal blade.

In the study described herein, a series of existing failure models were examined for suitability in predicting the onset of failure in selected single-crystal material specimens.[7–9] By observing how closely the various equations were able to correlate low-cycle fatigue (LCF) test data and by how well they reduced the scatter in the LCF data, we were able to assess their applicability in modeling the test data. The equation with the highest correlation was then used as the basis for a new single-crystal failure model for the SSME turbine blades. This new model was validated by comparing its predictions of stress concentration locations and relative magnitudes against empirical evidence of crack formation and growth in actual SSME turbine blades.

Overview of Current Failure Models

The majority of components and structures in service are generally subjected to multiaxial cyclic loading conditions resulting in biaxial and triaxial states of stress. Pressure vessels, turbine blades, drive shafts, crankshafts, and axles are common examples. To predict fatigue life of such components and structures using laboratory test data, a suitable multiaxial fatigue theory or criterion is required to relate complex stress states to laboratory data. Any fatigue failure criteria chosen must have the ability to account for high mean-stress effects. The LCF regime is characterized by crack formation and growth that is governed by the maximum shear-strain amplitude.

To be able to characterize failure onset and growth in a crystal material, it is first necessary to develop equations for local shear stresses and strains in each primary octahedral slip system.[10] Because a crystal material remains crystalline after slip, there are limitations on the number of ways a crystal material can slip. Often, but not always, slip in metal crystals occurs on planes of high atomic density in closely packed directions, where the distance between the atoms is minimum. The most probable slip planes and slip directions in metals depend on the crystal structure of the metal.

To model the failure of PWA 1480, two failure models were developed as a joint effort with Pratt and Whitney based on the resolved shear strain on the crystallographic planes including the effect of the strain normal to those planes, maximum shear strain, maximum normal strain, shear stress, and normal stress[11]:

$$(\gamma_{\max} + \varepsilon_{\max})/2 = f(N)_1 \tag{1}$$

$$\left(\left\{(\gamma_{\max} + \varepsilon_{\max})[180/(\lambda + 90)]^{0.5}\right\}/2\right) \times 100 = f(N)_2 \tag{2}$$

where

$$\lambda = \tan^{-1}(\gamma_{\max}/\varepsilon_{\max}) \times 180/\pi \tag{2a}$$

Brown and Miller[12] proposed that cracks initiate on the maximum shear plane and, therefore, suggested that the critical parameters governing fatigue life are the maximum shear strain and the strain normal to the plane of maximum shear strain. Kandil et al.[13] suggested the following convenient expression for this hypothesis for a given fatigue life:

$$\gamma_{\max} + S\varepsilon_{\max} = f(N)_3 \tag{3}$$

An alternative formulation of this critical shear-strain approach was proposed by Fatemi and Kurath,[14] which is expressed for a given fatigue life as

$$(\Delta\gamma_{\max}/2)[1 + k(\sigma_{\max\text{-}n}/\sigma_{ys})] = f(N)_4 \tag{4}$$

This model indicates that no shear direction crack growth occurs if there is no shear alternation.

Findley[15] proposed that the alternating shear stress is the primary cause of fatigue with the normal stress on the critical shear plane having a linear influence on the allowable alternating shear stress. Socie et al.[16] formulated the following equation based on Findley's hypothesis[15]:

$$\Delta\gamma_{\max}/2 + \Delta\varepsilon_n/2 + \sigma_n/E = f(N)_5 \tag{5}$$

This equation incorporates observed changes in crack closure for different stress and strain states. Finally, the strain energy density criterion can be written as follows[17]:

$$\tfrac{1}{2}(\sigma_x\varepsilon_x + \sigma_y\varepsilon_y + \sigma_z\varepsilon_z + \tau_{xy}\gamma_{xy} + \tau_{yz}\gamma_{yz} + \tau_{zx}\gamma_{zx}) = V_0 \tag{6}$$

Failure Model Assessment

The applicability of the failure models given by Eqs. (1–6) to the current problem was assessed in two ways. First, each model's usefulness was assessed on the basis of how well it was able to correlate and reduce the scatter in LCF data. Those models that exhibited the best data correlation were noted as possible candidates to be used in the development of an improved failure model for the SSME first-stage blade material. Next, the six failure models were evaluated using a finite element model of the SSME first-stage blade. Model predictions of failure-parameter values $f(N)_{1,\ldots,6}$ were obtained under realistic load and constraint conditions and at different material orientations. The results are presented as contour plots in terms of the various primary and secondary material orientations. These comparisons provided enough information for us to be able to identify which models warranted continued consideration in the development of an improved failure model.

Preliminary Assessment Using LCF Data

Strain-controlled LCF tests were conducted at 1200°F in air for PWA 1480 uniaxial smooth specimens using four loading directions (001, 111, 213, and 011). Figure 2 shows the crystallographic coordinate system with respect to the loading coordinate system for the single-crystal specimen used in the LCF tests. LCF strain range data were obtained in the loading coordinate system and are plotted

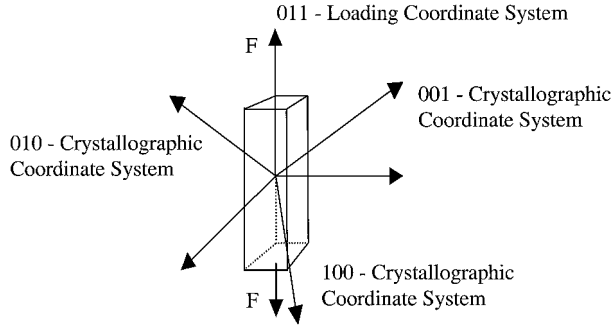

Fig. 2 LCF test specimen.

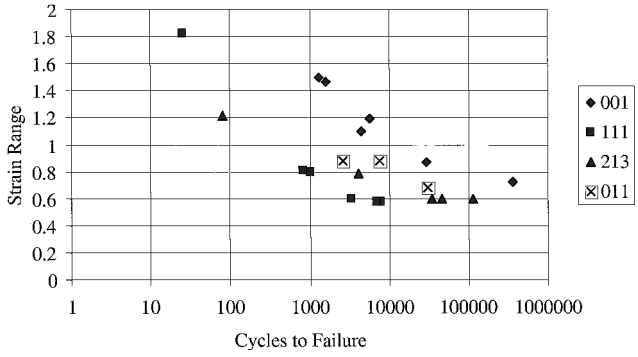

Fig. 3 PWA 1480 LCF strain data at 1200°F.

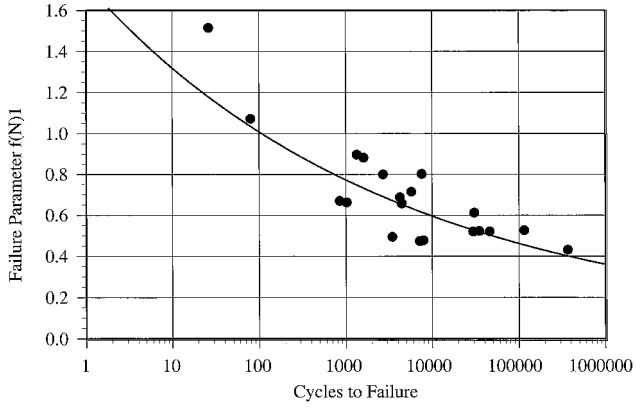

Fig. 4 Curve fitting the LCF test data using Eq. (1).

in Fig. 3 vs cycles to failure for the PWA 1480 single-crystal material. To assess the failure models given by Eqs. (1–6), stress values were found using the strain values in Fig. 3 after converting them to the material coordinate system. Next, by the use of the kinematic equations for crystallographic slip planes,[10] the maximum resultant shear strain and the strain normal to those planes were found.

For each failure model, failure parameters $f(N)_{1,\ldots,6}$ were calculated and plotted vs the number of cycles to failure (for example, see Fig. 4). A least-squares method was then used to find trendlines that would correlate the data in each case (Fig. 4). The correlation coefficients of these trendlines are given in Table 1. Based on the information in Table 1, Eqs. (2) and (3) stand out from all others by having the highest R^2 values. Therefore, it appears that after this initial examination, these two equations warrant further investigation and could be used in developing a failure criterion for single-crystal materials.

Table 1 Correlation coefficients R^2 for modified version of failure equations (1–6)

Failure model	R^2
Eq. (1)	0.679
Eq. (2)	0.823
Eq. (3)	0.858
Eq. (4)	0.714
Eq. (5)	0.769
Eq. (6)	0.593

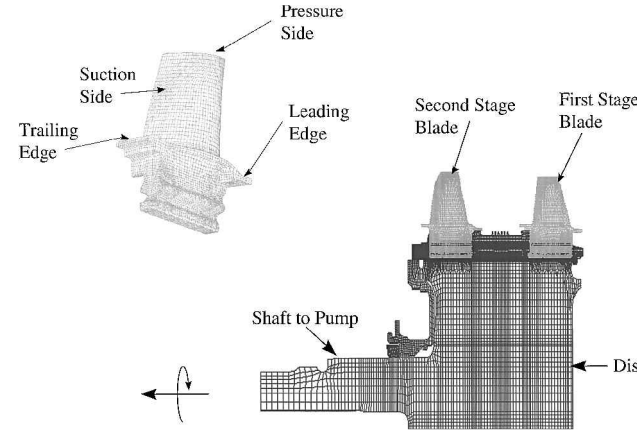

Fig. 5 Global finite element model used for first- and second-stage ATD/HPFTP blades.

Assessment Using Finite Element Models

Finite Element Model Description

The global finite element model of the ATD/HPFTP (developed using ANSYS[18] by ADAPCO for Pratt and Whitney) consists of the first- and second-stage blade, blade spacers, disk, and shaft (Fig. 5). The first- and second-stage blade models were built with eight-noded three-dimensional solid elements, that is, ANSYS SOILD45 elements. This particular element type allows the user to input the material properties in any orientation desired. As a result, it is ideally suited for analyzing the behavior of the single-crystal material considered in this study.

The ANSYS combination element is used as a gap element to simulate the interaction between the disk, blades, and the blade spacers during a steady-state analysis. This element is a combination of a spring-slider and damper in parallel, coupled to a gap in series. The total number of gap elements was 2200. They were divided into two groups, each with 1100 elements, that is, gap elements with large stiffness, and gap elements with small stiffness. The gap elements with large stiffness were carrying the load between the blade and the disk. The gap elements with small stiffness were closed springs and remained closed. The latter group of gap elements was used to provide solution stability.

A submodel was developed from the global model to represent the first stage-blade to reduce the run time associated with the full model. Boundary conditions were obtained in the form of displacements from the global model results file and were applied at the interface boundary nodes of the submodel. All pressure, mechanical, and thermal loads applied to the submodel were consistent with the global model.

The submodel consists of 28,734 elements and 33,572 nodes, that is, about 22% of the global model. Run times for the submodel are, therefore, significantly less than those of the global model. To assess the validity of the submodel, maximum principal stresses for both the baseline global model and the baseline submodel were calculated and compared. The loads and constraints in both models were developed to simulate a steady-state analysis at 109% service life. A centrifugal force, a thermal load, and a pressure load were applied to the global model as well as the submodel. The centrifugal load was applied as an angular velocity about a particular axis. A comparison between the principal stresses at a group of nodes for the global model and the submodel showed identical results, which verified the correctness and accuracy of the submodel.[11] A total of 297 orientations was considered to cover the total range of acceptable primary and secondary orientations within the first-stage single-crystal blade. These orientations will eventually be related

Table 2 Single-crystal material orientations modeled by ANSYS

Case no.	Δ, deg	γ, deg	θ, deg
0	0	0	0, 10, 20, 30, 40, 50, 60, 70, 80
1	7.5	0	0, 10, 20, 30, 40, 50, 60, 70, 80
2	6.93	2.87	0, 10, 20, 30, 40, 50, 60, 70, 80
3	5.3	5.3	0, 10, 20, 30, 40, 50, 60, 70, 80
4	2.87	6.93	0, 10, 20, 30, 40, 50, 60, 70, 80
5	0	7.5	0, 10, 20, 30, 40, 50, 60, 70, 80
6	−2.87	6.93	0, 10, 20, 30, 40, 50, 60, 70, 80
7	−5.3	5.3	0, 10, 20, 30, 40, 50, 60, 70, 80
8	−6.93	2.87	0, 10, 20, 30, 40, 50, 60, 70, 80
9	−7.5	0	0, 10, 20, 30, 40, 50, 60, 70, 80
10	−6.93	−2.87	0, 10, 20, 30, 40, 50, 60, 70, 80
11	−5.3	−5.3	0, 10, 20, 30, 40, 50, 60, 70, 80
12	−2.87	−6.93	0, 10, 20, 30, 40, 50, 60, 70, 80
13	0	−7.5	0, 10, 20, 30, 40, 50, 60, 70, 80
14	2.87	−6.93	0, 10, 20, 30, 40, 50, 60, 70, 80
15	5.3	−5.3	0, 10, 20, 30, 40, 50, 60, 70, 80
16	6.93	−2.87	0, 10, 20, 30, 40, 50, 60, 70, 80
17	15	0	0, 10, 20, 30, 40, 50, 60, 70, 80
18	13.86	5.74	0, 10, 20, 30, 40, 50, 60, 70, 80
19	10.6	10.6	0, 10, 20, 30, 40, 50, 60, 70, 80
20	5.74	13.86	0, 10, 20, 30, 40, 50, 60, 70, 80
21	0	15	0, 10, 20, 30, 40, 50, 60, 70, 80
22	−5.74	13.86	0, 10, 20, 30, 40, 50, 60, 70, 80
23	−10.6	10.6	0, 10, 20, 30, 40, 50, 60, 70, 80
24	−13.86	5.74	0, 10, 20, 30, 40, 50, 60, 70, 80
25	−15	0	0, 10, 20, 30, 40, 50, 60, 70, 80
26	−13.86	−5.74	0, 10, 20, 30, 40, 50, 60, 70, 80
27	−10.6	−10.6	0, 10, 20, 30, 40, 50, 60, 70, 80
28	−5.74	−13.86	0, 10, 20, 30, 40, 50, 60, 70, 80
29	0	−15	0, 10, 20, 30, 40, 50, 60, 70, 80
30	5.74	−13.86	0, 10, 20, 30, 40, 50, 60, 70, 80
31	10.6	−10.6	0, 10, 20, 30, 40, 50, 60, 70, 80
32	13.86	−5.74	0, 10, 20, 30, 40, 50, 60, 70, 80

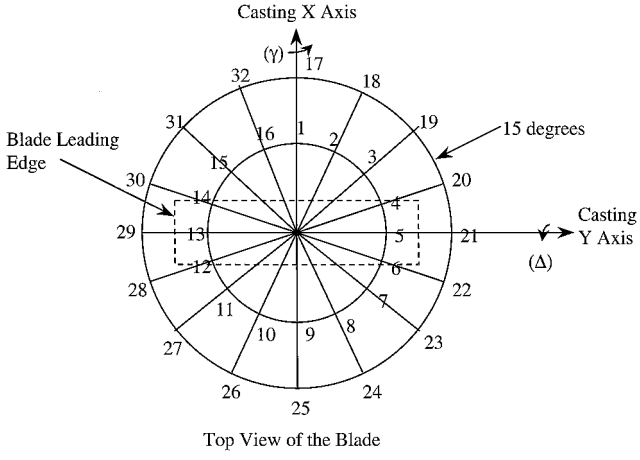

Fig. 6 Material Coordinate System, 297 orientations.

to the base crystallographic coordinate system that is used by the ANSYS model. Figure 6 together with Table 2 present all orientations that have been used in this analysis.

Comparison of Failure Models

When the failure model described Eq. (2) was applied to an ANSYS finite element model of the actual blade structure, a discontinuity was found at one of the two nodes of interest for the first-stage blade (Fig. 7). This discontinuity occurred because the failure parameter is automatically set to zero when the four normal octahedral strains are negative. Because of this discontinuity, the failure model given by Eq. (2) had to be modified. Because positive normal strain will help the material at the crack tip to experience all of the applied shear load, a conservative approach would be to consider only positive strain.[19] Therefore, rather than set the entire failure parameter $f(N)_2$ equal to a value of zero if all normal octahedral strains are negative, we propose that only the normal strain be set to zero. In this case $f(N)_2$ will be equal to one-half the maximum octahedral shear strain. When this modification was implemented in Eq. (2), the discontinuity was removed (Fig. 8). This modified version of Eq. (2) will be used in all following calculations and analyses.

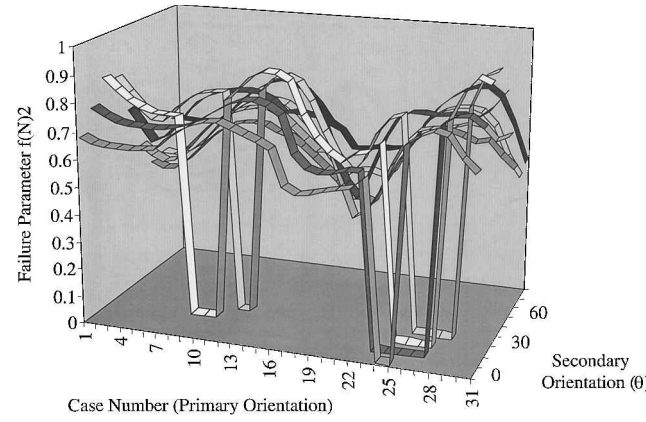

Fig. 7 Failure-parameter values given by Eq. (2).

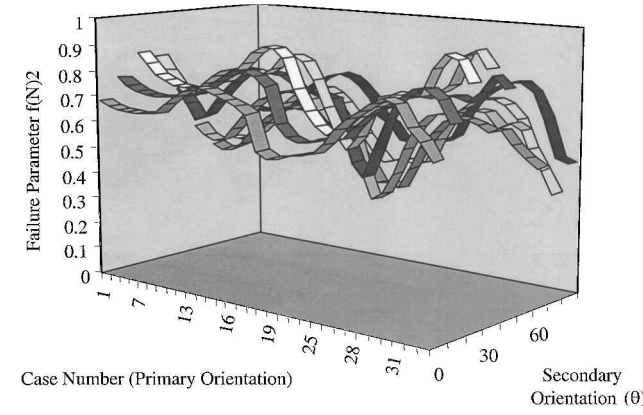

Fig. 8 Failure-parameter values given by modified version of Eq. (2).

Examination of the contour plots obtained using Eqs. (1–6) revealed that using Eqs. (2), (3), and (5) resulted in nearly identical failure-parameter contour distributions: Maximum and minimum values were found to occur at practically the same orientation angles. However, the contour plots obtained by using Eqs. (4) and (6) were significantly different. Based on these results, it is concluded that the failure models given by Eqs. (2) and (3) continue to warrant further consideration and could be used in developing an improved failure criterion.

Final Assessment

Note that, unlike the failure model given by Eq. (3), the modified failure model given by Eq. (2) does not require any predetermined constants. In addition, Eq. (2) also accounts for those cases where there are compressive or tensile normal strains because of the presence of a mode mixity term, whereas Eq. (3) does not. From these considerations and in light of its excellent correlation of the LCF test data, the modified version of failure Eq. (2) is considered to be the best candidate for a new single-crystal material failure model. In the next section, this new model is validated by comparing its predictions of crack growth locations against actual engine data. It is also used to investigate the influence of primary and secondary axis orientations on the behavior of single-crystal material.

Validation of Proposed Failure Model

A group of nodes at the tip of the first-stage blade submodel are selected for study based on the availability of engine test results and possible crack initiation. In addition, the calculations at these nodes will highlight the influence of the secondary axis orientations on the behavior of single-crystal materials. Contour plots of failure-parameter values will be compared with test data to validate the failure model given by the modified version of Eq. (2).

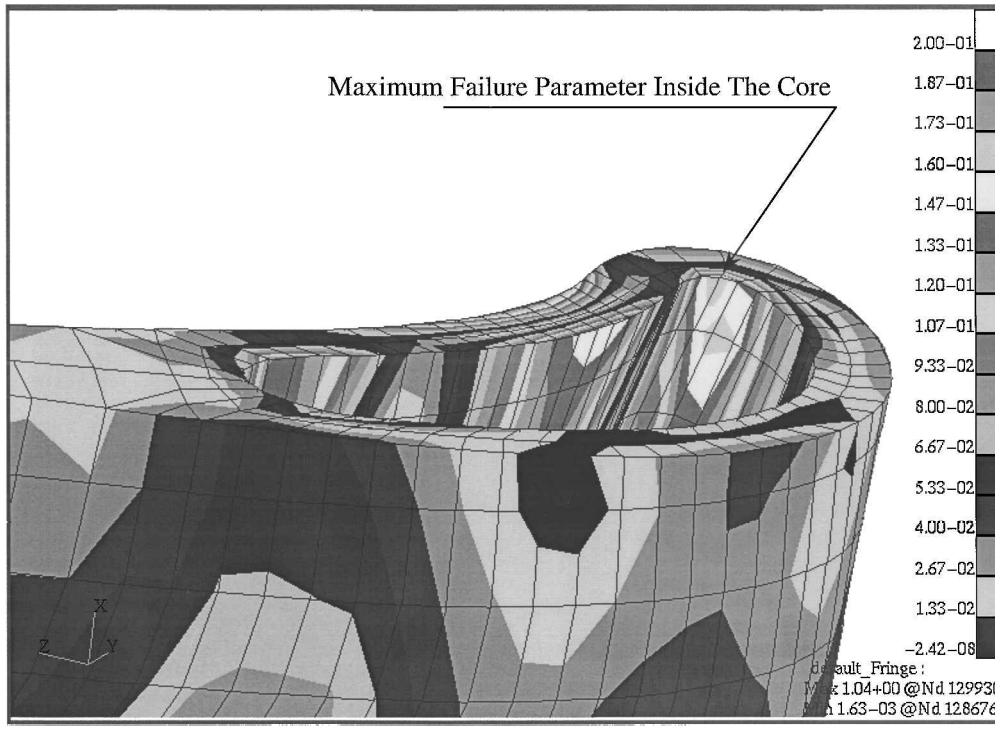

Fig. 9 Failure-parameter contour plot at the blade tip.

Figure 9 shows the failure-parameter contour plots at the tip of the first-stage single-crystalblade using the proposed failure model. Figure 9 shows that the maximum values of the failure parameter exist near the locations where the nodes were picked. Failure-parameter contour plots at tip nodes will be compared with the engine test results in more detail in the next section to see if the proposed failure model can be used to predict correctly the behavior of the single-crystal material and the failure of the SSME turbine blades.

Analytical Results

Contour plots were created using the proposed failure model and consisted of the failure-parameter values plotted against the primary and secondary axis orientations. Eight tip nodes were picked based on the engine test results and are possible locations for crack initiation. Figures 10a and 10b show the failure parameter values at tip nodes 124,675 and 123,739, respectively. By comparing the maximum and minimum parameter values in Figs. 10a and 10b, for example, it is evident that the failure parameter value could be made to vary by up to a factor of 3 by changing the primary and secondary material orientations. Figures 10a and 10b show that the highest failure-parameter values occur for cases 14 and 15 and for secondary orientation angles of $\theta = 0$–5 and 80–85 deg. The lowest failure parameter occurs for cases 0 and 9 and for a secondary orientation angle of $\theta = 50$ deg. In the failure-parameter contour plots, a higher failure-parameter value corresponds to a higher loading on the slip system, that is, the likely failure mechanism. A review of all of the contour plots revealed that the highest value of the failure parameter was at tip node 123,739. Therefore, node 123,739 was used in the comparison of the analytical and engine test results.

Engine Test Results

Engine test data comes from two ATD/HPFTP configurations (units F3–4B and F6–5D), which were tested on the SSME at NASA SSC. Both units experienced cracking of the airfoil tips in multiple blades, but only a few cracks grew all of the way across the wall of the hollow-core airfoil. The cracks that grew across the wall propagated down the length of the blade and in one case failed the blade, causing damage to the ATD/HPFTP and the SSME. Crack initiation was determined by NASA and Pratt and Whitney to be caused by faulty fabrication of the ceramic cores used in casting

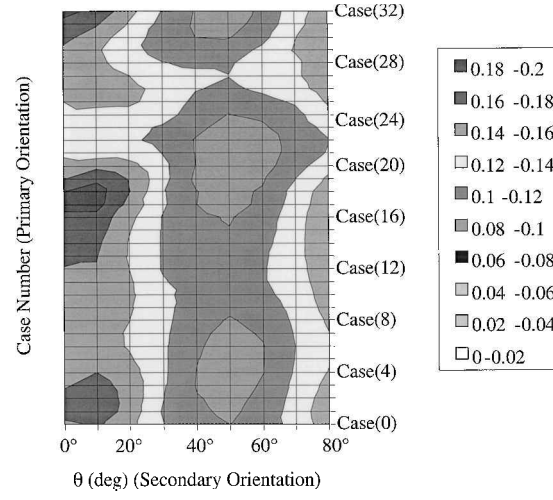

Fig. 10a Failure parameters at blade tip node 124,675.

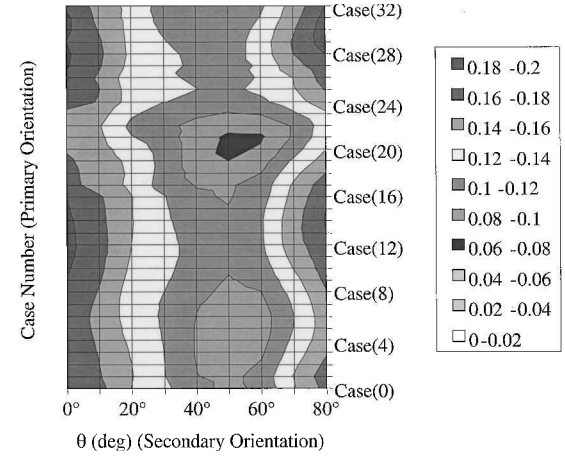

Fig. 10b Failure parameters at blade tip node 123,739.

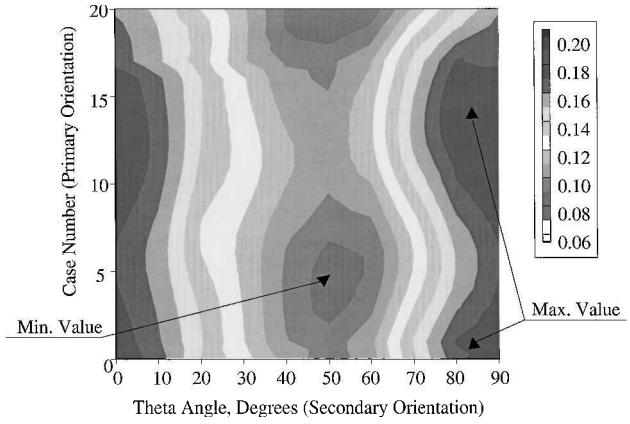

Fig. 11a Failure-parameter contour plot at blade tip node 123,739.

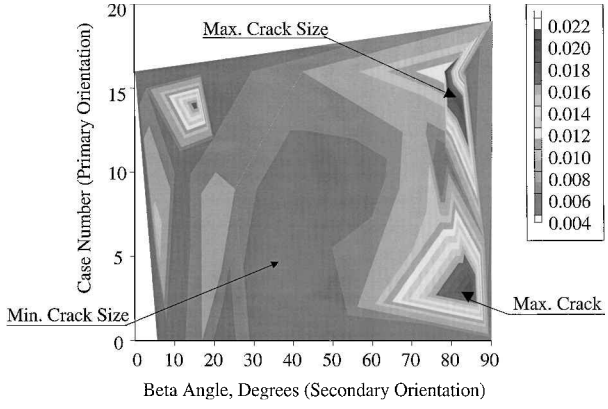

Fig. 11b Crack size contour plot at blade tip node 123,739.

the blades.[11] Specifically, rough edges on the cores were believed to have created stress concentrations. For this reason, blades with all orientations of material had cracks initiate, but only some of the blades propagated those cracks.

Figures 11a and 11b show the calculated failure parameter vs material orientation and a contour plot of experimental crack lengths in the blade vs material orientation, respectively. The darker shading in Fig. 11b corresponds to longer cracks; the cracks that grew through the wall are the darkest peaks. Figure 11a shows that the highest value of the failure parameter occurred for case 15 with a secondary orientation angle of $\theta = 85$ deg. This prediction agrees well with the test data in Fig. 11b, which shows that the longest crack length occurred for case 14 and with a secondary orientation angle of $\theta = 80$ deg. Figure 11a also shows that cracks would not be expected between cases 0 and 10 with a secondary orientation angle of $\theta = 45$ deg. This prediction also agrees with the test results in Fig. 11b, which shows that there are rarely cracks in the engine test data occurring between cases 0 and 10 with secondary orientation angle $\theta = 45$ deg.

These comparisons show a good correlation between the analytical predictions of peak failure-parameter value locations and the actual locations of blade cracking. In addition, the contour plots for both the analytical and experimental results show that the failure-parameter values changed with changes in the primary and secondary material orientations and that certain material orientations consistently gave low failure-parameter values. This is an important result with serious implications in manufacturing SSME blades using a single-crystal material. The failure parameter peaks can be avoided by forcing the primary and secondary axes to be within certain orientations in the casting process of the single-crystal material. Based on the analytical and engine test results, primary orientation angles of $\Delta = -2.87$ deg and $\gamma = 6.93$ deg together with a secondary orientation angle of $\theta = 45$ deg about the primary axis will give the lowest failure-parameter value for the system and material considered in this study.

Conclusions

The orientation of a single-crystal material are known to affect the strength and life of structural component parts. An analytical study has been performed using the first stage blade of the SSME to study the effects of secondary axis orientation angles on blade failure rate. This investigation first considered the correlation of different failure equations with LCF test data for single-crystal test specimens. Based on the results obtained, a new failure model was proposed. A comparison between the analytical results and the engine test results showed that the proposed failure model correlates well with test data and differentiates the blades that grew cracks through the wall thickness from those that did not. The comparison also demonstrated the dependence of blade stresses and cracking locations on crystal orientation.

Acknowledgments

This work was conducted under NASA Contract NAS8-40836. The authors wish to express their thanks to Jeff Rayburn of NASA Marshall Space Flight Center for his help and advice in the code modifications required for this work. The authors also wish to thank Gregory Swanson of NASA Marshall Space Flight Center.

References

[1]Chandler, W., "Materials for Advanced Rocket Engine Turbopump Turbine Blades," *Advanced High Pressure O_2/H_2 Technology*, edited by S. Morea and S. Wu, NASA CP-2372, 1985, pp. 110–132.

[2]Dreshfield, R., and Parr, R., "Application of Single-Crystal Superalloys for Earth-to-Orbit Propulsion Systems," AIAA Paper 87-1976, June 1987.

[3]Fritzemeier, L., "Advanced Single-Crystal for SSME Turbopumps," NASA CR-182244, 1989.

[4]Duhl, D., "Single-Crystal Superalloys," *Superalloys, Super Composites and Super Ceramics*, edited by J. Tien and T. Caufield, Academic Press, New York, 1989, pp. 149–182.

[5]Bowen, K., Nagy, P., and Parr, R., "The Evaluation of Single-Crystal Superalloys for Turbopump Blades in the SSME," AIAA Paper 86-1477, June 1986.

[6]Abdul-Aziz, A., August, R., and Nagpal, V., "Design Considerations for a Space Shuttle Main Engine SSME Turbine Blade Made of Single-Crystal Material," *Computers and Structures*, Vol. 46, No. 2, 1993, pp. 249–259.

[7]Lee, H., and Franck, C., "Analysis of Single-Crystal Turbine Blade for the Space Shuttle Main Engines," *ANSYS Conference Proceedings*, edited by D. E. Dietrich, Vol. 2, Swanson System, Inc., 1991, pp. 12.67–12.80.

[8]Kalluri, S., Aziz, A., and McGaw, M., "Elastic Response of [001]-Oriented PWA 1480 Single-Crystal—The Influence of Secondary Orientation," *SAE Transactions*, Vol. 100, Sec. 1, Pt. 1, Sept. 1997, pp. 273–283.

[9]Aziz, A., Kalluri, S., and McGaw, M., "The Influence of Primary and Secondary Orientations on the Elastic Response of a Nickel-Base Single-Crystal Superalloy," NASA TM-106125, April 1993.

[10]Stouffer, D., and Dame, L., *Inelastic Deformation of Metals*, Wiley, New York, 1996, Chap. 8.

[11]Sayyah, M. T., "A New Failure Criterion for Single-Crystal Metals as Used in the Space Shuttle Main Engine Turbine Blades," Ph.D. Dissertation, Mechanical and Aerospace Engineering Dept., Univ. of Alabama, Huntsville, AL, Aug. 1999.

[12]Brown, M., and Miller, K., "A Theory of Fatigue Under Multiaxial Stress-Strain Conditions," *Proceedings of the Institution of Mechanical Engineers*, Vol. 187, No. 65, 1973 pp. 745–755.

[13]Kandil, F., Brown, M., and Miller, K., "Biaxial Low-Cycle Fatigue of 316 Stainless Steel at Elevated Temperature," *Metal Society*, Vol. 280, 1982, pp. 203–210.

[14]Fatemi, A., and Kurath, P., "Multiaxial Fatigue Life Predictions Under the Influence of Mean-Stresses," *Journal of Engineering Materials and Technology*, Vol. 110, No. 4, 1988, pp. 380–388.

[15]Findley, W., "A Theory for the Effect of Mean Stress on Fatigue of Metals Under Combined Torsional and Axial Load of Bending," *Journal of Engineering Industry*, Vol. 81, Nov. 1959, pp. 301–306.

[16]Socie, D., Kurath, P., and Koch, J., "A Multiaxial Fatigue Damage Parameter," *Proceedings of the Second International Symposium on Multiaxial Fatigue*, 1985.

[17]Beer, F., and Johnston, E., *Mechanics of Materials*, McGraw–Hill, New York, 1981, Chap. 10.

[18]ANSYS Structural Program, Ver. 5.3, ANSYS, Inc., Houston, PA, 1996.

[19]Bannantine, J., Comer, J., and Handrock, J., *Fundamentals of Metal Fatigue Analysis*, Prentice–Hall, Upper Saddle River, NJ, 1990.

M. P. Nemeth
Associate Editor